

Confined concrete model of circular, elliptical and octagonal CFST short columns

Vipulkumar I. Patel ^{*1,4}, Brian Uy ^{2,4a}, Prajwal K.A. ^{3,4b} and Farhad Aslani ^{4,5c}

¹ School of Engineering and Mathematical Sciences, College of Science, Health and Engineering, La Trobe University, P.O. Box 199, Bendigo, VIC 3552, Australia

² School of Civil Engineering, The University of Sydney, Sydney, NSW 2006, Australia

³ Department of Civil Engineering, Indian Institute of Technology Bombay, Mumbai 400076, India

⁴ Centre for Infrastructure Engineering and Safety, School of Civil and Environmental Engineering, The University of New South Wales, Sydney, NSW 2052, Australia

⁵ School of Civil, Environmental and Mining Engineering, The University of Western Australia, Crawley, WA 6009, Australia

(Received February 23, 2016, Revised May 19, 2016, Accepted October 13, 2016)

Abstract. The confined concrete stress-strain curves utilised in computational models of concrete-filled steel tubular (CFST) columns can have a significant influence on the accuracy of the predicted behaviour. A generic model is proposed for predicting the stress-strain behaviour of confined concrete in short circular, elliptical and octagonal CFST columns subjected to axial compression. The finite element (FE) analysis is carried out to simulate the concrete confining pressure in short circular, elliptical and octagonal CFST columns. The concrete confining pressure relies on the geometric and material parameters of CFST columns. The post-peak behaviour of the concrete stress-strain curve is determined using independent existing experimental results. The strength reduction factor is derived for predicting the descending part of the confined concrete behaviour. The fibre element model is developed for the analysis of circular, elliptical and octagonal CFST short columns under axial loading. The FE model and fibre element model accounting for the proposed concrete confined model is verified by comparing the computed results with experimental results. The ultimate axial strengths and complete axial load-strain curves obtained from the FE model and fibre element model agree reasonably well with experimental results. Parametric studies have been carried out to examine the effects of important parameters on the compressive behaviour of short circular, elliptical and octagonal CFST columns. The design model proposed by Liang and Fragomeni (2009) for short circular, elliptical and octagonal CFST columns is validated by comparing the predicted results with experimental results.

Keywords: confined concrete model; numerical analysis; concrete-filled steel tubular columns

1. Introduction

Concrete-filled steel tubular (CFST) columns have been increasingly used in the high-rise buildings, bridges and port structures across the world. The constructional, structural, economic

*Corresponding author, Ph.D., Lecturer, E-mail: v.patel@latrobe.edu.au

^a Ph.D., Professor, E-mail: b.uy@unsw.edu.au

^b B.Tech. Student, E-mail: prajwalka@iitb.ac.in

^c Ph.D., Senior Lecturer, E-mail: farhad.aslani@uwa.edu.au

and environmental benefits of using CFST columns are well acknowledged by researchers (Shams and Saadeghvaziri 1997, Shanmugam and Lakshmi 2001, Spacone and El-Tawil 2004, Ellobody 2013, Han *et al.* 2014). Cold-formed circular and fabricated box sections are often utilised for the construction of CFST columns. Elliptical CFST column sections have recently been investigated for the structural applications. Both experimental and numerical studies have been carried out for predicting the behaviour of CFST columns. For numerical studies, finite element analysis (FEA) is often used for simulating the behaviour of CFST columns. The material constitutive models used in the FEA of CFST columns could have a significant influence on the accuracy of the predicted behaviour. Confined concrete models for circular, elliptical and octagonal CFST columns are proposed by researchers. However, discrepancies in the existing confined concrete models have been found. Therefore, the aim of this paper is to develop a generic confined concrete model for the accurate characterisation of the behaviour of circular, elliptical and octagonal CFST short columns under axial compression.

Extensive experimental and numerical studies have been undertaken for predicting the structural performance of CFST short columns under axial compression (Shams and Saadeghvaziri 1997, Shanmugam and Lakshmi 2001, Spacone and El-Tawil 2004, Ellobody 2013, Uy *et al.* 2011, Tao *et al.* 2013, Aslani *et al.* 2015a, b). O'Shea and Bridge (1998), Schneider (1998), Giakoumelis and Lam (2004), Sakino *et al.* (2004), Han *et al.* (2005) and Ren *et al.* (2014) tested circular CFST short columns under axial compression. Experimental studies indicated that the concrete confinement in circular CFST short columns increases both the strength and ductility of the concrete core (Klöppel and Goder 1957, Furlong 1967, Knowles and Park 1969). The concrete confinement in CFST columns is affected by the sectional shape (Susantha *et al.* 2001). The experimental studies on axially loaded elliptical CFST short columns are relatively limited (Yang *et al.* 2008, Zhao and Packer 2009, Jamaluddin *et al.* 2013, Uenaka 2014). Only Tomii *et al.* (1977) conducted tests on octagonal CFST short columns under axial loading.

Hence, the performance of CFST columns is affected by the sectional shape, diameter-to-thickness ratio, concrete compressive strengths and steel yield strengths. Experimental studies can be conducted to examine the effects of every parameter on the behaviour of CFST columns. However, experimental studies can be comparatively expensive. Numerical studies can be employed to conduct extensive parametric studies. These numerical studies depend on the accurate concrete confinement models for predicting reliable results. Tang *et al.* (1996), Susantha *et al.* (2001) and Hu *et al.* (2003) proposed concrete confinement models for circular CFST columns subjected to axial compression. It was found that these confinement models may underestimate or overestimate the concrete confinement in circular CFST columns as pointed out by Liang and Fragomeni (2009). Only Dai and Lam (2010) proposed a concrete confining pressure model for elliptical CFST short columns. Dai and Lam (2010) obtained good agreement between the numerical and experimental results. A design formula for predicting the ultimate axial strength of elliptical CFST short columns needs to be proposed. Susantha *et al.* (2001) proposed a confined concrete model for the concrete core confined by the octagonal steel tube in CFST columns. Their confined concrete model is modified in this paper based on the finite element analysis results.

As indicated by Liang and Fragomeni (2009), existing confined concrete models for circular CFST columns overestimate the confinement in high strength circular CFST columns. Liang and Fragomeni (2009) also indicated that there are discrepancies between these confined concrete models for circular CFST columns. It highlights that a generic concrete constitutive model is needed for circular, elliptical and octagonal CFST short columns. The confined concrete model for circular, elliptical and octagonal CFST short columns has been developed by Liang and Fragomeni

(2009), Dai and Lam (2010) and Susantha *et al.* (2001), respectively. This paper extends these different confined concrete models to a generic confined concrete model for circular, elliptical and octagonal CFST short columns under axial loading. The commercial FE program ABAQUS is employed to model circular, elliptical and octagonal CFST short columns under axial loading. A user-defined Python script has also been developed for the FE model of these CFST columns. The generic confined concrete model is then utilised for the nonlinear inelastic analysis of circular, elliptical and octagonal CFST short columns subjected to axial compression. Moreover, the design model proposed by Liang and Fragomeni (2009) is used to calculate the ultimate axial strengths of circular, elliptical and octagonal CFST short columns.

2. Finite element analysis

2.1 General concept

The cross-sections of CFST columns are depicted in Fig. 1. A Python script was developed for the FE model of axially loaded CFST short columns in ABAQUS. The main benefit of the developed Python script over the traditional CAE approach is to automatically generate many FE models based on the user inputs (Puri 2011). A sequentially uncoupled eigenvalue buckling-static general procedure was employed for the nonlinear inelastic analysis of CFST short columns. For sequentially uncoupled analysis, the computational results from an eigenvalue buckling analysis were utilised to account for the global imperfections in a static general analysis. The imperfections were assigned as the lowest buckling mode. The imperfection was considered as $L/1000$ (Tao *et al.* 2013).

CFST short columns were modelled using the ABAQUS FE program. The concrete core in CFST short columns under axial loading does not rotate and hence the 8-node linear brick reduced integration solid elements, C3D8R, can be used for modelling the deformation of the concrete core. The steel tube in CFST columns buckles locally outwards. Both the shell and solid elements capture the local buckling behaviour of the steel tube in CFST short columns. However, the large shell elements do not effectively mesh around the curved surface between the concrete and steel tube. Therefore, the steel tube was modelled using 8-node linear brick reduced integration solid elements (C3D8R). The concrete element size of 10 mm and steel element size of 5 mm were used for the present FE model (Dai and Lam 2010).

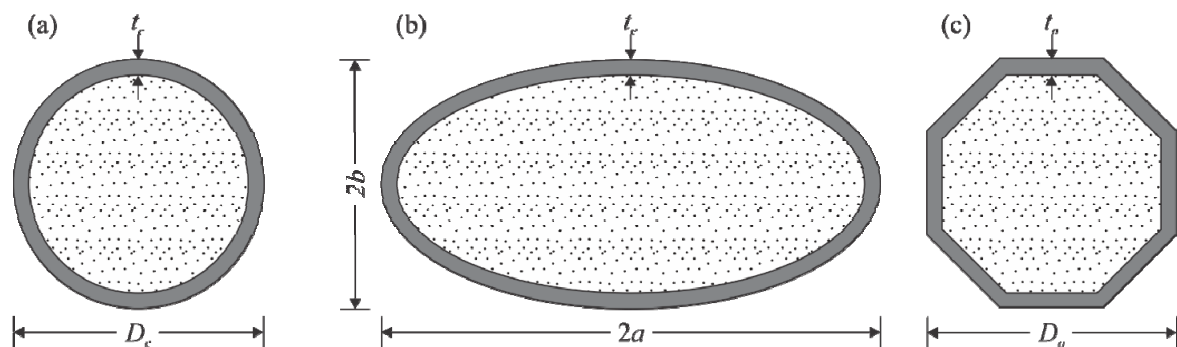


Fig. 1 Section shapes of CFST columns: (a) circular; (b) elliptical; and (c) octagonal

The interaction between the steel tube and concrete surface depends on the master-slave surface selection, sliding formulation, discretization methods and interaction properties. The finite sliding formulation allows the separation, sliding and rotation between the contact surfaces while the small sliding formulation allows a little sliding between the contact surfaces. It was found that the choice of the sliding formulation, finite sliding or small sliding, does not have a considerable effect on the behaviour of CFST short columns. The finite sliding formulation was considered in the present FE model for the interaction definition between the steel tube and concrete surface. The inner surface of a steel tube is taken as master surface while the outer surface of a concrete core acts as a slave surface. The penetration between the steel tube and concrete surface was restricted by using 'Hard Contact' in the normal direction. The tangential behaviour of the steel tube-concrete contact was simulated by selecting the penalty friction formulation. It was noted that the friction factor has a small effect on the behaviour of CFST short columns (Dai and Lam 2010). A friction factor of 0.25 was considered in the present FE model. CFST columns were fixed at the bottom while the top end was only allowed to displace in the loading direction. The FE models for CFST columns are presented in Fig. 2.

2.2 Material constitutive models

2.2.1 Structural steels

Mild structural steel, cold-formed steel or high-strength structural steel are generally utilised in the construction of CFST columns. The stress-strain curve for mild structural steel is characterised by a typical yield plateau. An idealised tri-linear stress-strain relationship was used for mild structural steel as illustrated in Fig. 3. The stress-strain curve of cold-formed steel shows a rounded stress-strain curve. The rounded stress-strain curve is replaced by a straight line for high strength steel as shown in Fig. 3. The rounded part of the stress-strain curve is expressed by the equation proposed by Liang (2009). In Fig. 3, σ_s represents the axial compressive steel stress, ε_s is the axial compressive steel strain, f_y denotes the steel yield strength, ε_y is the steel yield strain, ε_t is the hardening strain, f_{su} is the steel tensile strength and ε_{su} is the steel ultimate strain. The steel hardening strain (ε_t) is assumed to be 0.005 for cold-formed and high strength steels and $10\varepsilon_y$ for mild structural steel. The steel ultimate strain (ε_{su}) is taken as 0.2 (Liang 2009).

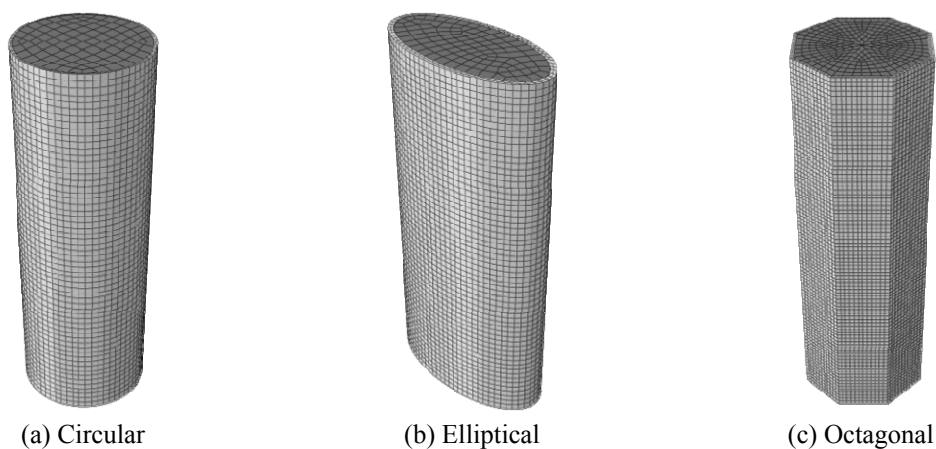


Fig. 2 Finite element model with meshing for concrete and steel components

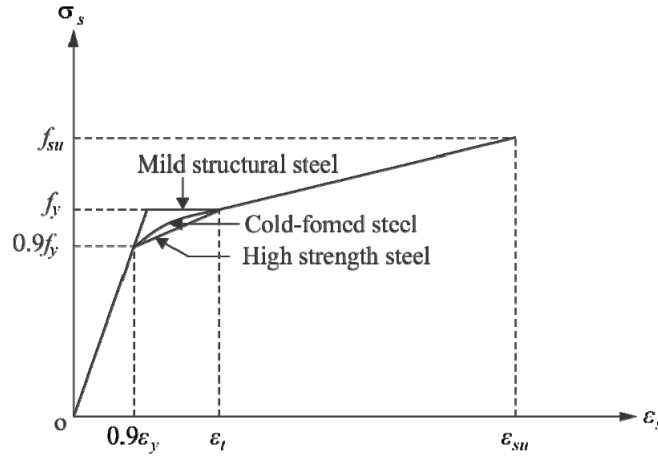


Fig. 3 Typical stress-strain curves for mild structural steel, cold-formed steel and high strength steel

2.2.2 Confined concrete

The concrete confinement provided by the encased steel tube in a circular, elliptical and octagonal CFST column increases the strength of the concrete core. The Drucker-Prager criterion is utilised for modelling the confined concrete in circular, elliptical and octagonal CFST columns. Tao *et al.* (2013) indicated that the confined concrete model is significantly affected by the material parameters such as angle of friction, flow-stress ratio and dilation angle. The sensitivity analysis was conducted to examine the effects of angle of friction, flow-stress ratio and dilation angle on the axial load-strain curves of CFST short columns under axial loading. Fig. 4 depicts the effects of angle of friction, flow-stress ratio and dilation angle on the axial load-strain curves of CFST short columns. The constant values of 20°, 0.8 and 0.001 are assumed for angle of friction, flow-stress ratio and dilation angle in defining the Drucker-Prager parameters based on sensitivity study. The typical stress-strain curves shown in Fig. 5 are employed in the FE model to represent the material behaviour of confined concrete in circular, elliptical and octagonal CFST columns.

The ascending first part OA of the stress-strain curve is simulated utilising the equations proposed by Mander *et al.* (1988) for confined concrete as follows

$$\sigma_c = \frac{f'_{cc} \lambda (\epsilon_c / \epsilon'_{cc})}{\lambda - 1 + (\epsilon_c / \epsilon'_{cc})^\lambda} \tag{1}$$

$$\lambda = \frac{E_c}{E_c - (f'_{cc} / \epsilon'_{cc})} \tag{2}$$

$$E_c = 3320 \sqrt{\gamma_c f'_c} + 6900 \quad (\text{MPa}) \tag{3}$$

in which σ_c represents the axial compressive concrete stress, ϵ_c denotes the axial compressive concrete strain, f'_{cc} is the axial compressive strength of concrete, ϵ'_{cc} is the compressive strain of confined concrete at f'_{cc} and E_c is the Young's modulus of concrete (ACI-318-11 2011).

It is found that the uniaxial compressive strength (f'_{cc}) and the corresponding ϵ'_{cc} of the confined

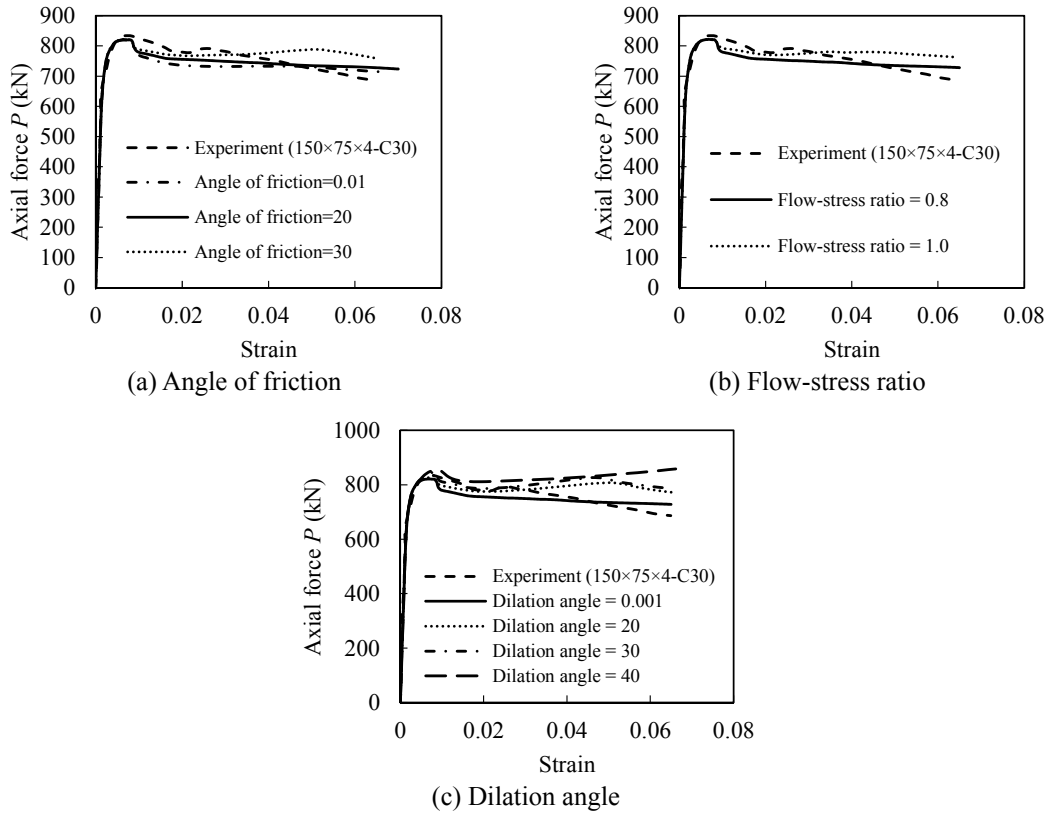


Fig. 4 Influence of angle of friction, flow-stress ratio and dilation angle on axial load-strain curves of CFST short columns

concrete core are much higher than those of the unconfined concrete core (Liang and Fragomeni 2009). The equations given by Mander *et al.* (1988) for the compressive strength and strain of confined concrete are modified by Liang and Fragomeni (2009) using the strength reduction factor γ_c as follows

$$f'_{cc} = \gamma_c f'_c + k_1 f_{rp} \quad (4)$$

$$\varepsilon'_{cc} = \varepsilon'_c \left(1 + k_2 f_{rp} / \gamma_c f'_c \right) \quad (5)$$

$$\gamma_c = 1.85 D_{cc}^{-0.135} \quad (0.85 \leq \gamma_c \leq 1.0) \quad (6)$$

in which f_{rp} represents the confining pressure on the concrete core, ε'_c is the strain at f'_c of unconfined concrete, D_{cc} is the diameter of the concrete core and k_1 and k_2 are constants which can be determined by experiments. Based on the study of Richart *et al.* (1928), k_1 and k_2 are respectively taken as 4.1 and 20.5 for circular and octagonal CFST columns. Dai and Lam (2010) indicated that k_1 is linearly varied with the aspect ratio (a/b) for elliptical CFST columns. The equation proposed by Dai and Lam (2010) for k_1 are modified here for elliptical CFST columns as follows

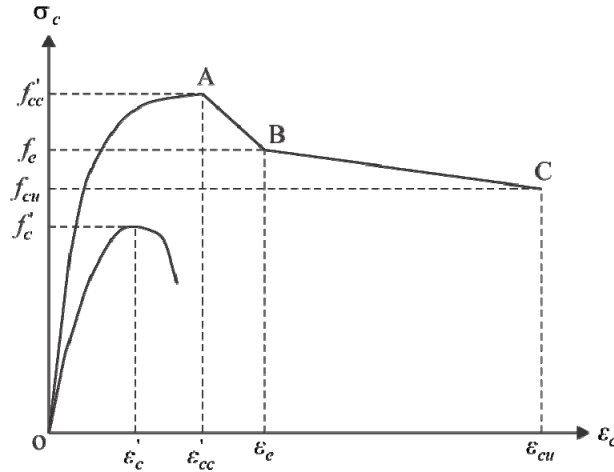


Fig. 5 A general stress-strain curve of concrete confined by circular, elliptical and octagonal steel tubes

$$k_1 = 6.7 - 2.6 \left(\frac{a}{b} \right) \tag{7}$$

The strain ϵ'_c is the strain at f'_c of unconfined concrete. The strain ϵ'_c was proposed by Liang and Fragomeni (2009) as follows

$$\epsilon'_c = \begin{cases} 0.002 & \text{for } \gamma_c f'_c \leq 28 \text{ (MPa)} \\ 0.002 + (\gamma_c f'_c - 28) / 54000 & \text{for } 28 < \gamma_c f'_c \leq 82 \text{ (MPa)} \\ 0.003 & \text{for } \gamma_c f'_c > 82 \text{ (MPa)} \end{cases} \tag{8}$$

The confining pressure relies on the steel yield strength and diameter-to-thickness ratio (Hu *et al.* 2003). Liang and Fragomeni (2009), Dai and Lam (2010) and Susantha *et al.* (2001) proposed the confined concrete models for circular, elliptical and octagonal CFST short columns, respectively. The confined concrete model for circular CFST short columns was developed by Liang and Fragomeni (2009) based on the diameter-to-thickness ratio range between 17 and 102. The confining pressure formulas proposed by Liang and Fragomeni (2009) are modified using the extensive experimental data with diameter-to-thickness ratio range from 17 to 221. The confined concrete model for elliptical CFST short columns has been proposed by Dai and Lam (2010). This model is modified by incorporating the additional experimental results (Yang *et al.* 2008 and Jamaluddin *et al.* 2013). The extensive experimental results are used to calibrate the confined concrete model. The lateral confining pressures obtained from the FE model are given in Tables 1, 2 and 3. The lateral confining pressure is obtained by the linear regression analysis from FE results and experimental data. The stress-strain relationship for confined concrete depicted in Fig. 5 is used in the finite element model to determine the lateral confining pressure. The lateral confining pressures obtained from the FE model are presented in Fig. 6. The equations for determining the lateral confining pressure on the concrete core for circular, elliptical and octagonal CFST short column are proposed here.

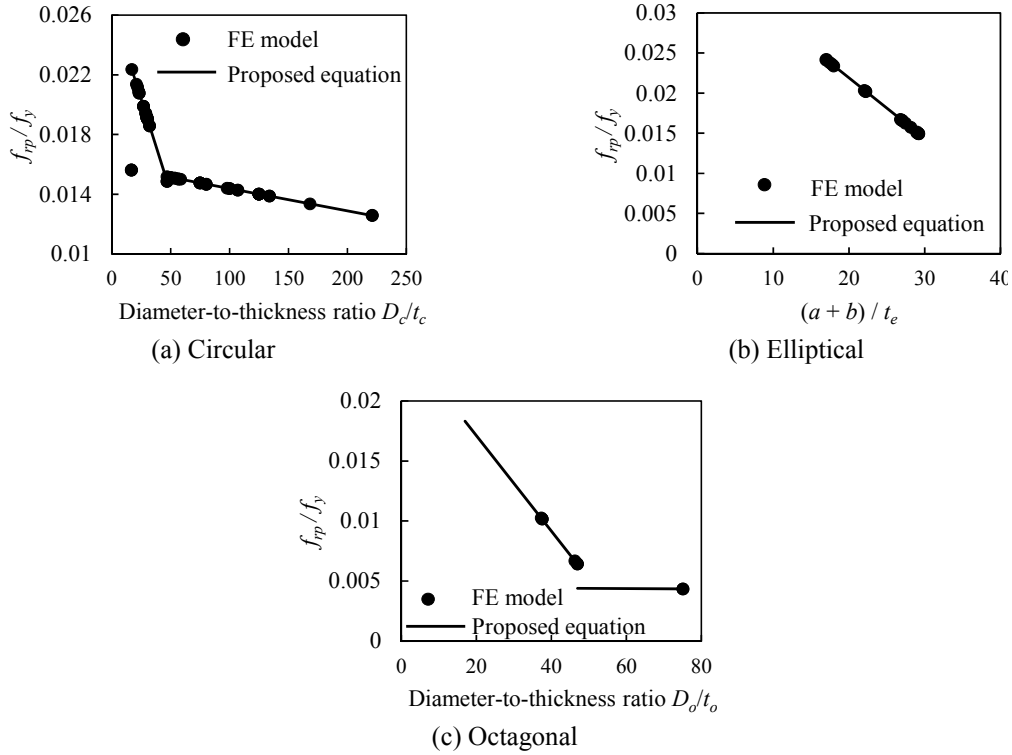


Fig. 6 Lateral confining pressures obtained from the FE model for circular, elliptical and octagonal CFST columns

For circular CFST columns

$$f_{rp} = \begin{cases} (0.02663 - 0.0002504 D_c/t_c) f_y & \text{for } 17 < D_c/t_c < 47 \\ (0.01588 - 0.0000149 D_c/t_c) f_y & \text{for } 47 \leq D_c/t_c \leq 221 \end{cases} \quad (9)$$

For elliptical CFST columns

$$f_{rp} = (0.037 - 0.000755(a+b)/t_e) f_y \quad \text{for } 17 \leq (a+b)/t_e \leq 29 \quad (10)$$

For octagonal CFST columns

$$f_{rp} = \begin{cases} (0.02508 - 0.0003977 D_o/t_o) f_y & \text{for } 17 < D_o/t_o < 47 \\ (0.004465 - 0.0000015 D_o/t_o) f_y & \text{for } D_o/t_o \geq 47 \end{cases} \quad (11)$$

in which D_c represents the diameter of circular cross-section, t_c denotes the thickness of circular steel tube, a is the major-axis radius of elliptical cross-section, b is the minor-axis radius of elliptical cross-section, t_e is the thickness of elliptical steel tube, D_o is the diameter of octagonal cross-section and t_o is the thickness of octagonal steel tube. These geometric parameters are shown

in Fig. 1. Eqs. (9)-(11) have been derived by the linear regression analysis from the results obtained from the FE model and the experimental data given in Tables 1-3. Eq. (10) was developed based on the experimental data with $(a + b)/t_e$ ratio less than 29.

Two linear lines AB and BC of the stress-strain curve for confined concrete as shown in Fig. 5 can be expressed by

$$\sigma_c = \begin{cases} f'_{cc} + (f_e - f'_{cc})(\varepsilon_c - \varepsilon'_{cc})/(\varepsilon_e - \varepsilon'_{cc}) & \text{for } \varepsilon'_{cc} < \varepsilon_c \leq \varepsilon_e \\ f_e + (f_{cu} - f_e)(\varepsilon_c - \varepsilon_e)/(\varepsilon_{cu} - \varepsilon_e) & \text{for } \varepsilon_e < \varepsilon_c \leq \varepsilon_{cu} \end{cases} \quad (12)$$

in which ε_e and ε_{cu} are concrete compressive strains at points B and C as depicted in Fig. 5. The compressive strain ε_e is taken as $10\varepsilon'_c$ corresponding to point B. The compressive strain ε_{cu} at point C is taken as $30\varepsilon'_c$. In Eq. (12), f_e is the stress corresponding to strain ε_e and f_{cu} represents the compressive stress at strain ε_{cu} . The stresses f_e and f_u are given by

$$f_e = \alpha_c f'_{cc} \quad (13)$$

$$f_u = \beta_c f'_{cc} \quad (14)$$

where the factors α_c and β_c represent the confinement effect on the concrete ductility in the post-peak range. These factors depend on the strength of concrete (Dai and Lam 2010). The factors are proposed for circular, elliptical and octagonal CFST short columns as

For circular CFST short columns

$$\alpha_c = \begin{cases} 0.8987 - 0.00122 \gamma_c f'_c & \text{for } \gamma_c f'_c < 50 \text{ MPa} \\ 0.774 - 0.0016 \gamma_c f'_c & \text{for } \gamma_c f'_c \geq 50 \text{ MPa} \end{cases} \quad (15)$$

$$\beta_c = \begin{cases} \alpha_c - 0.1 & \text{for } \gamma_c f'_c < 50 \text{ MPa} \\ 0.4 & \text{for } \gamma_c f'_c \geq 50 \text{ MPa} \end{cases} \quad (16)$$

For elliptical CFST short columns

$$\alpha_c = 0.889 - 0.004 \gamma_c f'_c \quad (17)$$

$$\beta_c = 0.841429 - 0.005714 \gamma_c f'_c \quad (18)$$

For octagonal CFST short columns

$$\alpha_c = 0.9729 - 0.0091 \gamma_c f'_c \quad (19)$$

$$\beta_c = 0.9987 - 0.0107 \gamma_c f'_c \quad (20)$$

3. Fibre element model

A general confined concrete model is first proposed by utilising the FE model for circular, elliptical and octagonal CFST short columns under axial loading. The confining pressure model is

then implemented in the fibre element model for the nonlinear inelastic analysis of circular, elliptical and octagonal CFST short columns under axial loading.

The fibre element methodology is an accurate and reliable analysis technique for simulating the performance of steel-concrete cross-sections (Liang and Fragomeni 2009, Patel *et al.* 2014). However, this methodology has not been employed for simulating the behaviour of elliptical CFST short columns under axial loading. This paper utilises the fibre element method for the nonlinear inelastic analysis of axially loaded CFST short columns. The elliptical cross-section is discretised using DistMesh code for creating the unstructured triangular meshes (Persson and Strang 2004). The discretization of circular cross-section proposed by Liang and Fragomeni (2009) is used for the analysis of circular CFST short columns. An octagonal CFST column is discretised into concrete and steel fibre elements. The discretization of circular, elliptical and octagonal CFST column sections is depicted in Fig. 7. After the discretization of CFST cross-sections, steel and concrete properties are assigned to fibre elements. The material stress-strain curves are utilized to determine fibre stresses from fibre strains. The stress resultant in the cross-section provides the axial forces. The internal axial compression carried by circular, elliptical and octagonal CFST column cross-sections under axial loading is predicted as stress resultants by numerical integration. The fibre element analysis is stopped when the predicted axial compression is below $0.5P_{\max}$. The analysis is also terminated when the strain attains the user-defined ultimate strain ε_{cu} (Liang 2009, 2014, Patel *et al.* 2015).

4. Verification

4.1 Ultimate axial strengths

Tables 1-3 provide details of the material properties, geometry and test results of circular, elliptical and octagonal CFST short columns under axial loading. It can be seen from Tables 1-3 that the FE model and fibre element model accurately predict the ultimate axial strengths of circular, elliptical and octagonal CFST short columns under axial compression. For circular section, the ratio of the mean ultimate axial strength predicted by the FE model to the experimental value is 0.98 with the standard deviation of 0.07 and the coefficient of variation of 0.07. The mean ultimate axial strength ($P_{u,FIB}$) predicted by the fibre element model to the experimental value ($P_{u,exp}$) is 1.03. Both standard deviation and coefficient of variation for $P_{u,FIB}/P_{u,exp}$ are 0.07. For elliptical section, the mean value of the computational to the experimental ultimate axial strength ($P_{u,FEA}/P_{u,exp}$) is

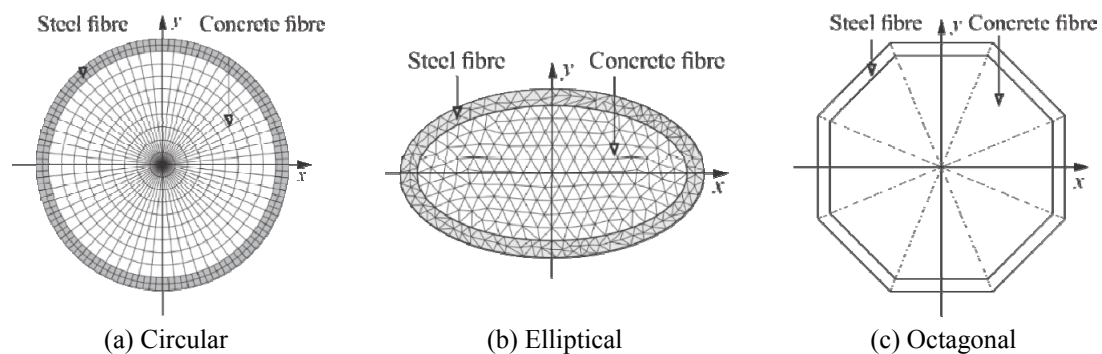


Fig. 7 Fibre element discretization of CFST column sections

0.99 with a standard deviation of 0.06 and a coefficient of variation of 0.06. The ratio of the mean ultimate axial strength predicted by the fibre element model to the experimental value is 1.00. Both the standard deviation and coefficient of variation are 0.06. For octagonal section, the ratio of the mean ultimate axial strength predicted by the FE model to the experimental value is 1.00 with the standard deviation of 0.04 and coefficient of variation of 0.04. It is observed from Table 3 that the mean ultimate axial strength predicted by the fibre model to the experimental value is 0.99. The standard deviation of $P_{u.FIB}/P_{u.exp}$ is 0.05 and coefficient of variation is 0.05.

Table 1 Ultimate axial strengths of axially loaded circular CFST short columns

Specimens	$D_c \times t_c$ (mm)	D_c/t_c	L (mm)	f_y (MPa)	E_s (GPa)	f'_c (MPa)	f_{rp} (MPa)	$P_{u.exp}$ (kN)	$P_{u.FEA}$ (kN)	$\frac{P_{u.FEA}}{P_{u.exp}}$	$P_{u.FIB}$ (kN)	$\frac{P_{u.FIB}}{P_{u.exp}}$	Ref.
S10CS50A	190×0.86	221	659.0	210.7	177.0	41.0	2.65	1350	1314	0.97	1452	1.08	O'Shea and Bridge (1998)
S12CS50A	190×1.13	168	664.5	185.7	178.4	41.0	2.48	1377	1288	0.94	1442	1.05	
S16CS50B	190×1.52	125	664.5	306.1	207.4	48.3	4.29	1695	1754	1.03	1970	1.16	
S20CS50A	190×1.94	98	663.5	256.4	204.7	41.0	3.70	1678	1603	0.96	1725	1.03	
S30CS50B	165×2.82	59	580.5	363.3	200.6	48.3	5.45	1662	1743	1.05	1868	1.12	
C1	140.8×3.00	47	605.4	285	189.475	28.180	4.24	881	973	1.10	1002	1.14	Schneider (1998)
C2	141.4×6.50	22	608.0	313	206.001	23.805	6.63	1825	1574	0.86	1525	0.84	
C3	140.0×6.68	21	616.0	537	205.322	28.180	11.48	2715	2472	0.91	2468	0.91	
C3	114.43×3.98	29	300.0	343	200	26.69	6.66	948	961	1.01	956	1.01	Giakoumelis and Lam (2004)
C4	114.57×3.99	29	300.0	343	200	79.56	6.67	1308	1086	0.83	1421	1.09	
C7	114.88×4.91	23	300.5	365	200	29.50	7.58	1380	1156	0.84	1145	0.83	
C8	115.04×4.92	23	300.0	365	200	89.16	7.58	1787	1310	0.73	1658	0.93	
C9	115.02×5.02	23	300.5	365	200	48.96	7.63	1413	1328	0.94	1325	0.94	
C11	114.29×3.75	30	300.0	343	200	48.96	6.52	1067	1095	1.03	1120	1.05	
C12	114.30×3.85	30	300.0	343	200	27.12	6.58	998	942	0.94	942	0.94	
C14	114.54×3.84	30	300.0	343	200	84.1	6.57	1359	1102	0.81	1444	1.06	
CC6-A-2	122×4.54	27	366.0	576	228	25.4	11.46	1509	1601	1.06	1692	1.12	Sakino <i>et al.</i> (2004)
CC6-A-4-1	122×4.54	27	366	576	228	40.5	11.46	1657	1738	1.05	1837	1.11	
CC6-A-4-2	122×4.54	27	366	576	228	40.5	11.46	1663	1738	1.05	1837	1.10	
CC8-A-2	108×6.47	17	324	853	228	25.4	13.33	2275	2240	0.98	2524	1.11	
CC8-A-4-1	109×6.47	17	327	853	228	40.5	13.33	2446	2355	0.96	2656	1.09	
CC8-A-4-2	108×6.47	17	324	853	228	40.5	13.33	2402	2329	0.97	2622	1.09	
CA1-1	60×1.87	32	180	282	207	72.42	5.24	312	319	1.02	330	1.06	Han <i>et al.</i> (2005)
CA1-2	60×1.87	32	180	282	207	72.42	5.24	320	319	1.00	330	1.03	
CA2-1	100×1.87	53	300	282	207	72.42	4.25	822	808	0.98	816	0.99	
CA2-2	100×1.87	53	300	282	207	72.42	4.25	845	808	0.96	816	0.97	
CA3-1	150×1.87	80	450	282	207	72.42	4.14	1701	1638	0.96	1679	0.99	
CA3-2	150×1.87	80	450	282	207	72.42	4.14	1670	1638	0.98	1679	1.01	
CA4-1	200×1.87	107	600	282	207	72.42	4.03	2783	2786	1.00	2815	1.01	

Table 1 Continued

Specimens	$D_c \times t_c$ (mm)	D_c/t_c	L (mm)	f_y (MPa)	E_s (GPa)	f'_c (MPa)	f_{rp} (MPa)	$P_{u,exp}$ (kN)	$P_{u,FEA}$ (kN)	$\frac{P_{u,FEA}}{P_{u,exp}}$	$P_{u,FIB}$ (kN)	$\frac{P_{u,FIB}}{P_{u,exp}}$	Ref.
CA4-2	200×1.87	107	600	282	207	72.42	4.03	2824	2786	0.99	2815	1.00	Han <i>et al.</i> (2005)
CA5-1	250×1.87	134	750	282	207	72.42	3.92	3950	4175	1.06	4210	1.07	
CA5-2	250×1.87	134	750	282	207	72.42	3.92	4102	4175	1.02	4210	1.03	
CB1-1	60×2	30	180	404	207	72.72	7.72	427	390	0.91	405	0.95	
CB1-2	60×2	30	180	404	207	72.42	7.72	415	390	0.94	404	0.97	
CB2-1	100×2	50	300	404	207	72.42	6.11	930	970	1.04	955	1.03	
CB2-2	100×2	50	300	404	207	72.42	6.11	920	970	1.05	955	1.04	
CB3-1	150×2	75	450	404	207	72.42	5.96	1870	1863	1.00	1931	1.03	
CB3-2	150×2	75	450	404	207	72.42	5.96	1743	1863	1.07	1931	1.11	
CB4-1	200×2	100	600	404	207	72.42	5.81	3020	3150	1.04	3206	1.06	
CB4-2	200×2	100	600	404	207	72.42	5.81	3011	3150	1.05	3206	1.06	
CB5-1	250×2	125	750	404	207	72.42	5.66	4442	4701	1.06	4764	1.07	
CB5-2	250×2	125	750	404	207	72.42	5.66	4550	4701	1.03	4764	1.05	
CC1-1	60×2	30	180	404	207	76.5	7.72	432	400	0.93	414	0.96	
CC1-2	60×2	30	180	404	207	76.5	7.72	437	400	0.92	414	0.95	
CC2-1	150×2	75	450	404	207	76.5	5.96	1980	1926	0.97	1995	1.01	
CC2-2	150×2	75	450	404	207	76.5	5.96	1910	1926	1.01	1995	1.04	
CC3-1	250×2	125	750	404	207	76.5	5.66	4720	4872	1.03	4934	1.05	
CC3-2	250×2	125	750	404	207	76.5	5.66	4800	4872	1.02	4934	1.03	
cc1-1	165×2.92	57	595	389.3	206	52.19	5.85	1904	1882	0.99	2029	1.07	
cc1-2	165×2.92	57	595	389.3	206	52.19	5.85	1984	1882	0.95	2029	1.02	
Mean										0.98	1.03		
Standard deviation (SD)										0.07	0.07		
Coefficient of variation (COV)										0.07	0.07		

Table 2 Ultimate axial strengths of axially loaded elliptical CFST short columns

Specimens	$2a \times 2b \times t_e$ (mm)	$\frac{a+b}{t_e}$	L (mm)	f_y (MPa)	E_s (GPa)	f'_c (MPa)	f_{rp} (MPa)	$P_{u,exp}$ (kN)	$P_{u,FEA}$ (kN)	$\frac{P_{u,FEA}}{P_{u,exp}}$	$P_{u,FIB}$ (kN)	$\frac{P_{u,FIB}}{P_{u,exp}}$	Ref.
150×75×4-C30	150.40×75.60 ×4.18	27	300	376.5	217.5	31.4	6.25	839	820	0.98	838	1.00	Yang <i>et al.</i> (2008)
150×75×4-C60	150.57×75.52 ×4.19	27	300	376.5	217.5	50.8	6.26	974	962	0.99	975	1.00	
150×75×4-C100	150.39×75.67 ×4.18	27	300	376.5	217.5	83.6	6.24	1265	1197	0.95	1208	0.95	
150×75×5-C30	150.12×75.65 ×5.12	22	300	369.0	217.1	31.4	7.51	981	944	0.96	946	0.96	

Table 2 Continued

Specimens	$2a \times 2b \times t_e$ (mm)	$\frac{a+b}{t_e}$	L (mm)	f_y (MPa)	E_s (GPa)	f'_c (MPa)	f_{rp} (MPa)	$P_{u,exp}$ (kN)	$P_{u,FEA}$ (kN)	$\frac{P_{u,FEA}}{P_{u,exp}}$	$P_{u,FIB}$ (kN)	$\frac{P_{u,FIB}}{P_{u,exp}}$	Ref.
150×75×5-C60	150.23×75.74×5.08	22	300	369.0	217.1	50.8	7.46	1084	1073	0.99	1072	0.99	Yang et al. (2008)
150×75×5-C100	150.28×75.67×5.09	22	300	369.0	217.1	83.6	7.47	1296	1297	1.00	1296	1.00	
150×75×6.3-C30	148.78×75.45×6.32	18	300	400.5	216.5	31.4	9.45	1193	1162	0.97	1154	0.97	
150×75×6.3-C60	148.92×75.56×6.43	17	300	400.5	216.5	50.8	9.54	1280	1301	1.02	1290	1.01	
150×75×6.3-C100	149.53×75.35×6.25	18	300	400.5	216.5	83.6	9.38	1483	1487	1.00	1478	1.00	
C1-150-C30	150.10×75.00×4.10	27	300	424.4	201.0	40.0	6.91	900	923	1.03	956	1.06	Jamaluddin et al. (2013)
C1-150-C60	150.20×75.10×4.00	28	300	424.4	201.0	52.8	6.68	1139	1001	0.88	1032	0.91	
C1-150-C100	150.10×75.20×4.20	27	299	424.4	201.0	90.0	7.11	1239	1299	1.05	1324	1.07	
C1-200-C30	197.8×100.1×5.10	29	398	361.7	209.0	41.1	5.41	1232	1421	1.15	1447	1.17	
C1-200-C60	197.8×100.1×5.10	29	398	361.7	209.0	56.5	5.41	1737	1606	0.92	1633	0.94	
C1-200-C100	197.4×100.1×5.10	29	398	361.7	209.0	98.4	5.42	2116	2116	1.00	2135	1.01	
Mean										0.99	1.00		
Standard deviation (SD)										0.06	0.06		
Coefficient of variation (COV)										0.06	0.06		

Table 3 Ultimate axial strengths of axially loaded octagonal CFST short columns

Specimens	D_o (mm)	t_o (mm)	L (mm)	$\frac{D_o}{t_o}$	f_y (MPa)	E_s (GPa)	f'_c (MPa)	f_{rp} (MPa)	$P_{u,exp}$ (kN)	$P_{u,FEA}$ (kN)	$\frac{P_{u,FEA}}{P_{u,exp}}$	$P_{u,FIB}$ (kN)	$\frac{P_{u,FIB}}{P_{u,exp}}$	Ref.
2HN	150	2.0	300	75	341.3	206	30.1	1.49	989	946	0.96	942	0.95	Tomii et al. (1977)
3HN	150	3.2	300	47	300.2	206	30.1	1.93	1094	1095	1.00	1088	0.99	
4HN	150	4.0	300	38	294.3	203	30.1	2.99	1316	1263	0.96	1251	0.95	
2MN	150	2.0	300	75	341.3	206	21.9	1.49	771	813	1.05	807	1.05	
3MN	150	3.2	300	47	300.2	206	21.9	1.93	916	966	1.05	957	1.04	
4MN	150	4.0	300	38	294.3	203	21.9	2.99	1193	1136	0.95	1121	0.94	
3LN	148	3.2	300	46	300.2	206	16.7	2.01	856	885	1.03	875	1.02	
4LN	149	4.0	300	37	294.3	203	16.7	3.02	1117	1074	0.96	1039	0.93	
Mean											1.00	0.99		
Standard deviation (SD)											0.04	0.05		
Coefficient of variation (COV)											0.04	0.05		

4.2 Axial load-strain curves

The FE model and fibre element model were utilised to predict the axial load-strain curves of specimens tested by Han *et al.* (2005). Fig. 8 compares the predicted axial load-strain curves with the experimental results for circular CFST short columns. It can be seen from Fig. 8 that the axial load-strain curves predicted by the FE model and fibre element model agree reasonably well with the experimental results. The initial stiffness of the axial load-strain curves predicted by the models agrees well with the experimental results. The models tend to accurately predict the ultimate axial strength of tested circular CFST short columns. However, the experimental curve slightly departs from the computational one after the ultimate axial strength. The discrepancy between computational and experimental results is due mainly to the uncertainty of the actual concrete compressive strength and stiffness and elastic modulus of steel.

The axial load-strain curves for elliptical CFST short columns obtained from the FE model and fibre element model are compared with the test results given by Yang *et al.* (2008). Fig. 9 presents the comparisons of experimental and computational results for six elliptical CFST short columns. It can be seen from Fig. 9 that the axial load-strain curves obtained from the FE model and fibre element model are consistent with the experimental results. The average elastic modulus of steel is utilised in the numerical models, which leads the deviations between the axial load-strain curves in elastic range. The axial load-strain curves predicted by the models slightly deviate from the experimental ones in the post-peak range. The use of the average concrete compressive strength in the models often tends to deviate the predicted behaviour from the experimental results.

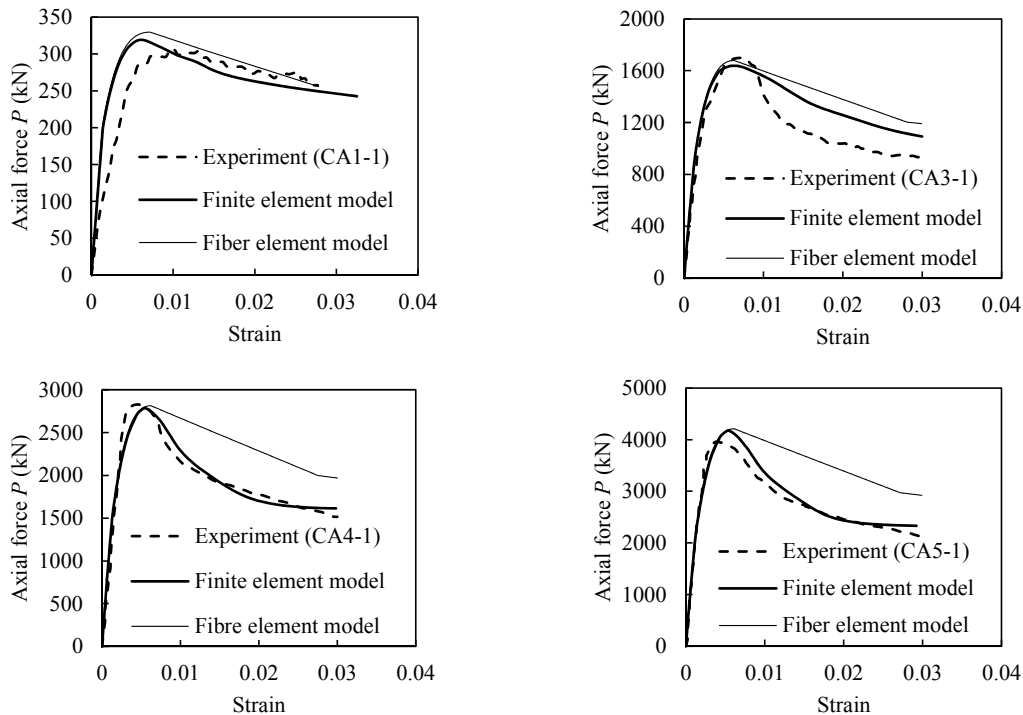


Fig. 8 Comparison of predicted and experimental axial load-strain curves for circular CFST short columns under axial compression

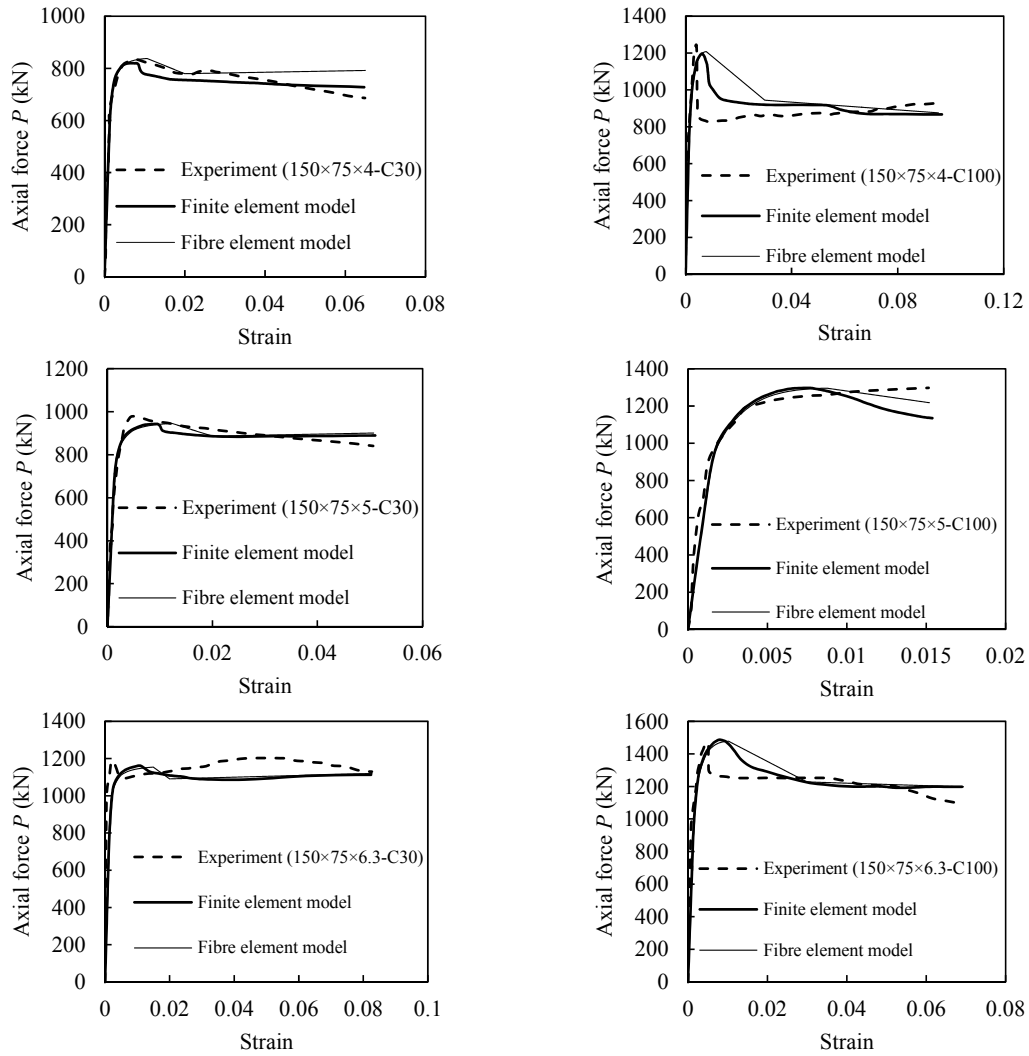


Fig. 9 Comparison of predicted and experimental axial load-strain curves for elliptical CFST short columns under axial compression

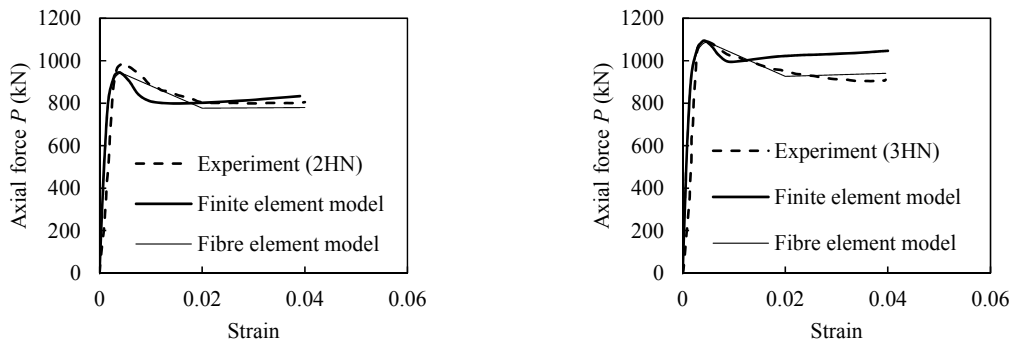


Fig. 10 Comparison of computational and experimental axial load-strain curves for octagonal CFST short columns under axial compression

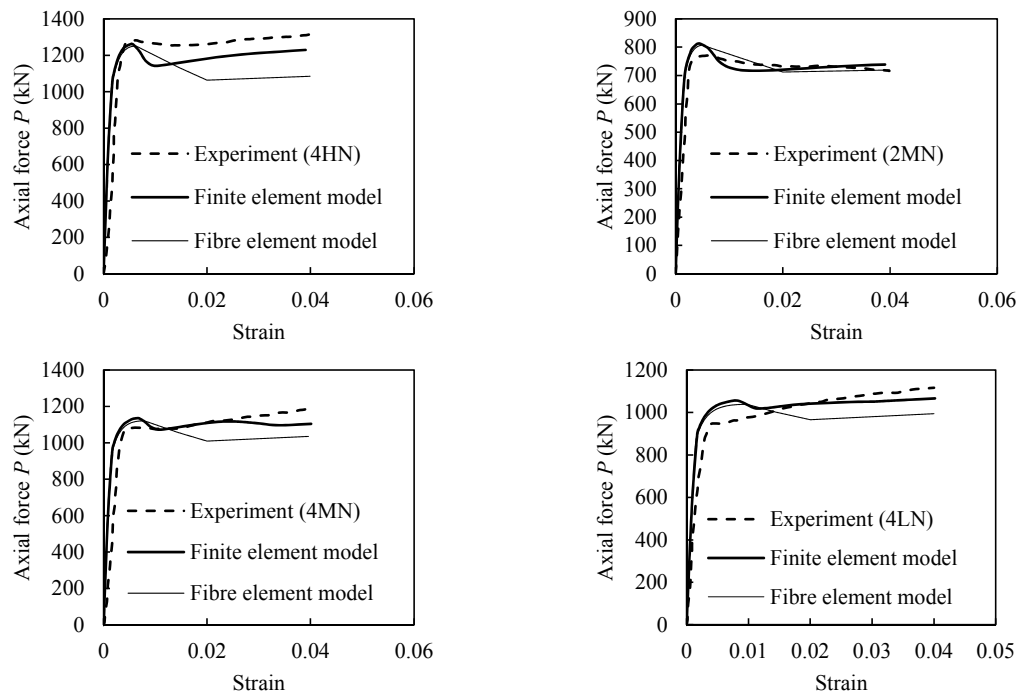


Fig. 10 Continued

Fig. 10 illustrates a comparison of computational and experimental axial load-strain curves for octagonal CFST short columns tested by Tomii *et al.* (1977). It can be seen from Fig. 10 that the axial load-strain curves predicted by the FE model and fibre element model agree reasonably well with the experimental results. The initial stiffness of the axial load-strain curves obtained from the models is slightly higher than that of the experimental results. This deviation is due to the uncertainty of the actual concrete stiffness and strength and elastic modulus of structural steels.

5. Parametric study

The behaviour of axially loaded CFST short columns is affected by diameter-to-thickness ratio, steel yield strength and concrete compressive strength. The verified fibre element model is utilized for examining the effects of depth-to-thickness ratio, steel yield strength and concrete compressive strength on the behaviour of circular, elliptical and octagonal CFST short columns under axial loading.

5.1 Effects of diameter-to-thickness ratio

The diameter-to-thickness ratio is one of the parameters affecting the concrete confinement offered by the encased steel tube regardless of the sectional shapes. The steel contribution to the ultimate axial strength of CFST columns is also affected by the diameter-to-thickness ratio. This is mainly due to the steel area varies with the diameter-to-thickness ratio. The diameter-to-thickness ratio was considered by changing the thickness of steel tube while maintaining the same cross-

section size. Circular columns C12, C13 and C15 (Table 4), elliptical columns E1, E12 and E13 (Table 5) and octagonal columns O1, O2 and O3 (Table 6) were analysed to examine the effects of diameter-to-thickness ratio on their behaviour.

The influence of diameter-to-thickness ratio on the axial load-strain curves for CFST short columns is presented in Fig. 11. It can clearly be seen from Fig. 11 that increasing the diameter-to-thickness ratio decreases the ultimate axial strength regardless of the sectional shape. The steel contribution to ultimate axial strength of CFST columns increases with an increase in the steel tube thickness for the same cross-section area. It should be noted that reducing the diameter-to-thickness ratio increases the steel area of the column cross-section. When increasing the diameter-to-thickness ratio from 40 to 50 and 100, the ultimate axial strength of circular CFST short columns decreases by 8.9% and 23.5%, respectively. For axially loaded elliptical CFST short columns, an increase in the diameter-to-thickness ratio $(a+b)/t_e$ from 19 to 23 and 28 decreases the ultimate axial strength by 8.3% and 17.4%, respectively. An increase in diameter-to-thickness ratio of octagonal CFST short columns from 37.5 to 50 and 75 decreases the ultimate axial strength by 24.0% and 36.8%, respectively.

5.2 Effects of steel yield strength

The strength and ductility of CFST columns are significantly influenced by the yield strength of the encased steel tube regardless of the sectional shape. The verified fibre element model was

Table 4 Comparison of ultimate axial strength of circular CFST short columns

Specimens	D_c (mm)	t_c (mm)	$\frac{D_c}{t_c}$	f_y (MPa)	f_u (MPa)	E_s (GPa)	f'_c (MPa)	$P_{u.FIB}$ (kN)	$P_{u.design}$ (kN)	$\frac{P_{u.design}}{P_{u.FIB}}$
C1	100	2	50	360	450	200	20	530	525	0.99
C2	100	2	50	360	450	200	25	566	561	0.99
C3	100	2	50	360	450	200	32	616	612	0.99
C4	100	2	50	360	450	200	40	674	669	0.99
C5	100	2	50	360	450	200	50	746	742	0.99
C6	100	2	50	360	450	200	65	854	850	1.00
C7	100	2	50	360	450	200	80	962	959	1.00
C8	100	2	50	360	450	200	100	1107	1103	1.00
C9	250	2	125	350	450	200	80	4848	4792	0.99
C10	250	2	125	450	520	200	80	5277	5206	0.99
C11	250	2	125	690	790	200	80	6310	6198	0.98
C12	500	12.5	40	450	520	200	50	21617	21650	1.00
C13	500	10	50	450	520	200	50	19697	19573	0.99
C14	500	6.25	80	450	520	200	50	17369	17095	0.98
C15	500	5	100	450	520	200	50	16532	16240	0.98
Mean										0.99
Standard deviation (SD)										0.01
Coefficient of variation (COV)										0.01

Table 5 Comparison of ultimate axial strengths of elliptical CFST short columns

Specimens	$2a$ (mm)	$2b$ (mm)	t_e (mm)	$\frac{a+b}{t_e}$	f_y (MPa)	f_u (MPa)	E_S (GPa)	f'_c (MPa)	$P_{u.FIB}$ (kN)	$P_{u.design}$ (kN)	$\frac{P_{u.design}}{P_{u.FIB}}$
E1	150	75	4	28	350	450	200	65	1001	999	1.00
E2	150	75	4	28	450	520	200	65	1155	1153	1.00
E3	150	75	4	28	690	790	200	65	1528	1523	1.00
E4	200	100	5	30	450	520	200	20	1409	1400	0.99
E5	200	100	5	30	450	520	200	25	1468	1461	1.00
E6	200	100	5	30	450	520	200	32	1551	1547	1.00
E7	200	100	5	30	450	520	200	40	1648	1644	1.00
E8	200	100	5	30	450	520	200	50	1770	1767	1.00
E9	200	100	5	30	450	520	200	65	1953	1950	1.00
E10	200	100	5	30	450	520	200	80	2136	2134	1.00
E11	200	100	5	30	450	520	200	100	2380	2379	1.00
E12	150	75	5	23	350	450	200	65	1110	1107	1.00
E13	150	75	6	19	350	450	200	65	1211	1206	1.00
Mean											1.00
Standard deviation (SD)											0.00
Coefficient of variation (COV)											0.00

Table 6 Comparison of ultimate axial strengths of octagonal CFST short columns

Specimens	D_o (mm)	t_o (mm)	$\frac{D_o}{t_o}$	f_y (MPa)	f_u (MPa)	E_S (GPa)	f'_c (MPa)	$P_{u.FIB}$ (kN)	$P_{u.design}$ (kN)	$\frac{P_{u.design}}{P_{u.FIB}}$	
O1	150	2	75	450	520	200	25	1000	1000	1.00	
O2	150	3	50	450	520	200	25	1203	1203	1.00	
O3	150	4	37.5	450	520	200	25	1583	1580	1.00	
O4	150	3	50	350	450	200	20	945	945	1.00	
O5	150	3	50	450	520	200	20	1122	1122	1.00	
O6	150	3	50	690	790	200	20	1549	1547	1.00	
O7	150	2	75	350	450	200	20	787	787	1.00	
O8	150	2	75	350	450	200	25	869	870	1.00	
O9	150	2	75	350	450	200	32	985	987	1.00	
O10	150	2	75	350	450	200	70	1617	1621	1.00	
Mean											1.00
Standard deviation (SD)											0.00
Coefficient of variation (COV)											0.00

employed to examine the influence of the steel yield strength on the compressive behaviour of circular, elliptical and octagonal CFST short columns under axial loading. Circular columns C9, C10 and C11 (Table 4), elliptical columns E1, E2 and E3 (Table 5) and octagonal columns O4, O5 and O6 (Table 6) were modelled to examine the effects of steel yield strength on their behaviour.

Fig. 12 depicts the influence of steel yield strength on the behaviour of circular, elliptical and octagonal CFST short columns under axial loading. It can be observed from Fig. 12 that the initial axial stiffness of CFST columns is not affected by steel yield strength regardless of the sectional shape. In contrast, the ultimate axial strength is significantly affected by steel yield strength. It was found that the ductility of CFST columns decreases with increasing the steel yield strength. This is because of the brittle nature of high strength steel. The ductility of CFST column section is defined by the ability of a section to undergo the plastic deformation without strength degradation (Liang and Fragomeni 2009). An increase in the steel yield strength considerably increases the ultimate axial strength of a CFST column. When increasing the steel yield strength from 350 MPa to 450 MPa and 690 MPa for circular CFST columns, the ultimate axial strength is increased by 8.8% and 30.1%, respectively. Increasing the steel yield strength from 350 MPa to 450 MPa and 690 MPa for elliptical CFST short columns increases the ultimate axial strength by 15.4% and 52.6%, respectively.

An increase in the steel yield strength from 350 MPa to 450 MPa and 690 MPa for octagonal

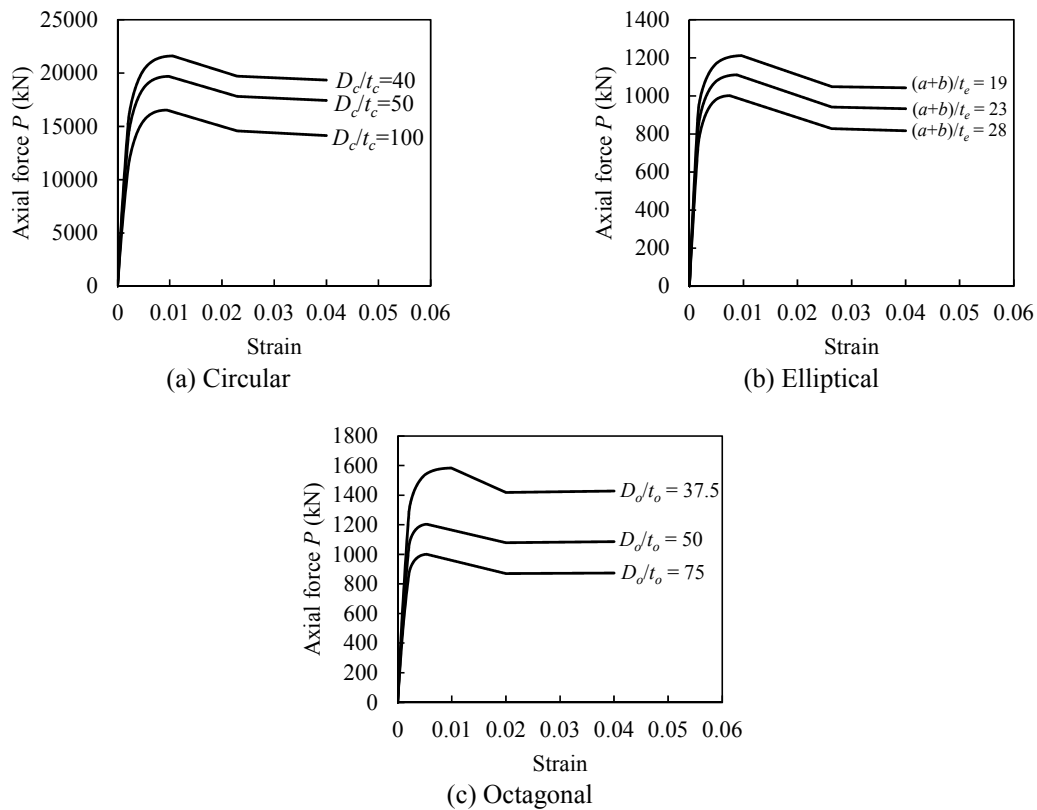


Fig. 11 Effects of diameter-to-thickness ratio on the behaviour of CFST short columns

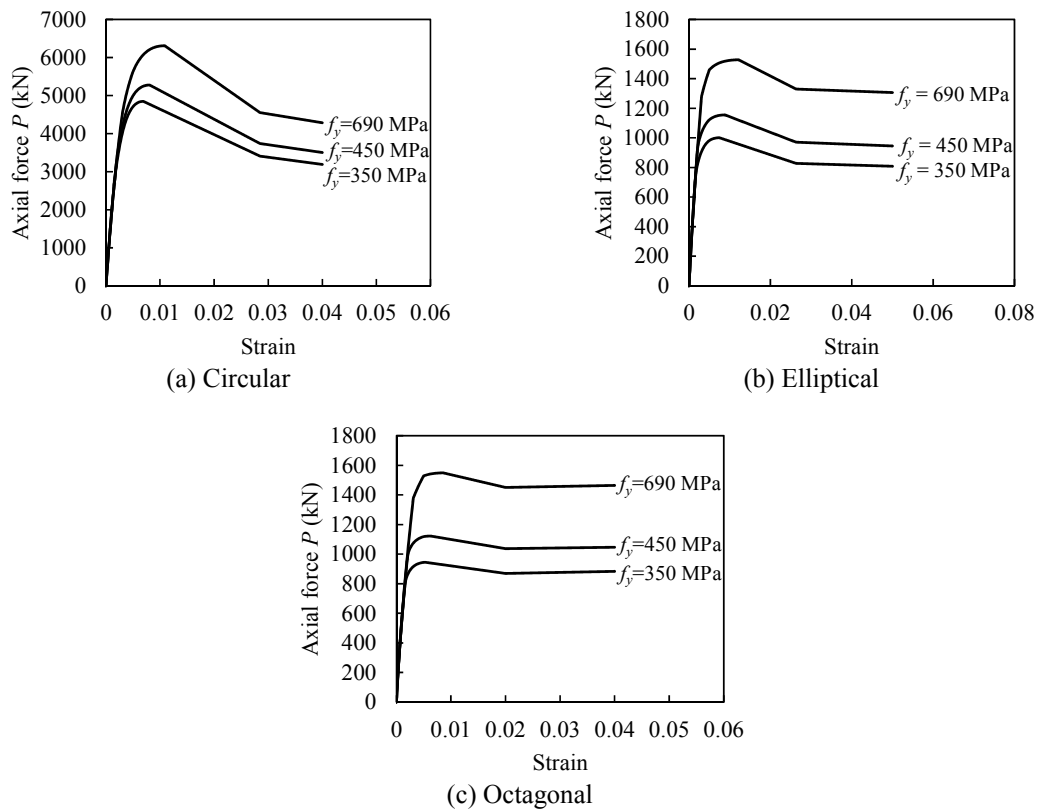


Fig. 12 Effects of steel yield strength on the behaviour of CFST short column

CFST short columns increases the ultimate axial strength by 18.8% and 64.0%, respectively.

5.3 Effects of concrete compressive strength

The influence of concrete compressive strength on the predicted behaviour of circular, octagonal and elliptical CFST short columns was investigated herein. Circular columns C3, C6 and C8 (Table 4), elliptical columns E7, E9 and E11 (Table 5) and octagonal columns O7 and O10 (Table 6) were analysed to investigate the effects of concrete compressive strength on their behaviour.

The influence of concrete compressive strength on the axial load-strain curves of circular, elliptical and octagonal CFST short columns is illustrated in Fig. 13. The ultimate axial strength of axially loaded CFST short columns increases with an increase in the concrete compressive strength regardless of the cross-sectional shape. For circular CFST columns, an increase in the concrete compressive strength from 32 MPa to 65 MPa and 100 MPa, the ultimate axial strength is increased by 38.7% and 79.7%, respectively. When increasing the concrete compressive strength from 40 MPa to 65 MPa and 100 MPa for elliptical CFST columns, the ultimate axial strength is increased by 18.4% and 44.4%, respectively. For octagonal CFST short columns, increasing the concrete compressive strength from 20 MPa to 70 MPa, the ultimate axial strength is increased by 51.3%.

6. Design model

The ultimate axial strength of circular, elliptical and octagonal CFST short columns subjected to axial compression depends on the material and geometric properties. It also relies on the concrete confinement offered by the encased steel tube. A design equation was proposed by Liang and Fragomeni (2009) for predicting the ultimate axial strength of axially loaded circular CFST short columns. The design equation given by Liang and Fragomeni (2009) is utilised for determining the ultimate axial strength of circular, elliptical and octagonal CFST short columns. The design equation is given as follows

$$P_{u.design} = (\gamma_c f'_c + k_1 f_{rp}) A_c + \gamma_s f_y A_s \tag{21}$$

in which f_{rp} is calculated by Eqs. (9), (10) and (11) for circular, elliptical and octagonal cross-sectional shapes, and γ_s stands for the strength factor for the steel tube, which is taken as 1.0 for elliptical and octagonal CFST short columns. For circular CFST columns, Liang and Fragomeni (2009) proposed the equation as follows

$$\gamma_s = 1.458(D_c/t_c)^{-0.1} \quad (0.9 \leq \gamma_s \leq 1.1) \tag{22}$$

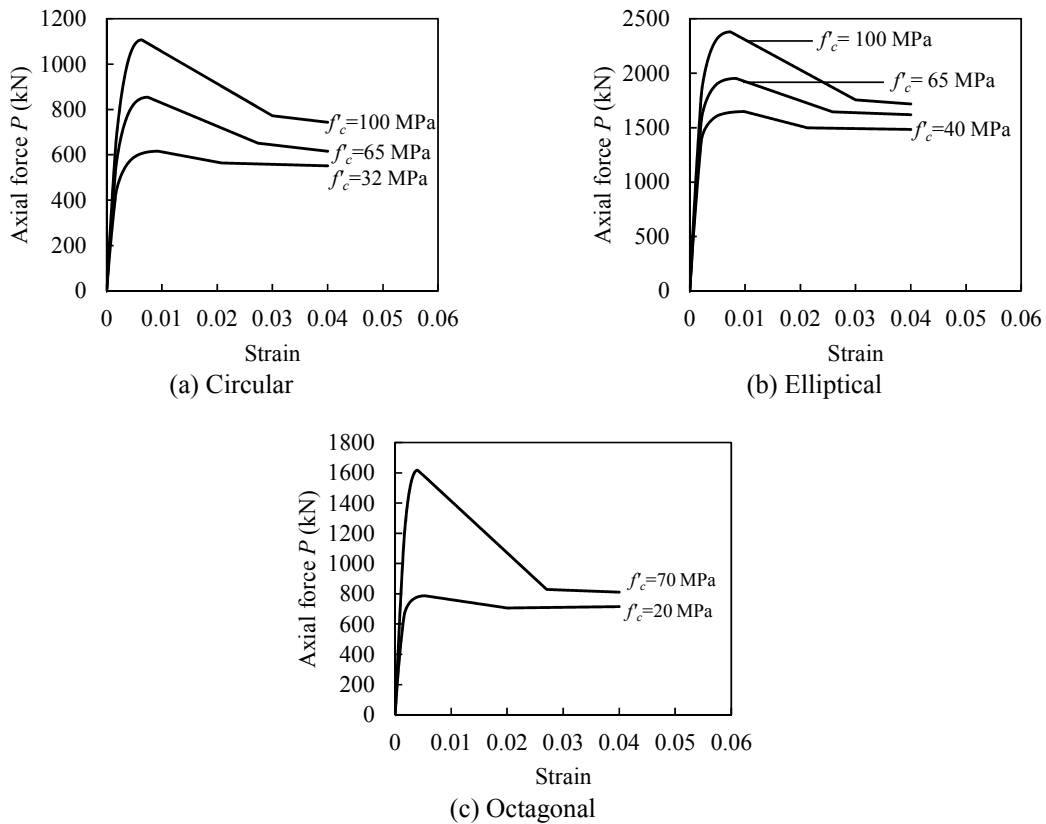


Fig. 13 Effects of concrete compressive strength on the behaviour of CFST short columns

The material and geometric parameters of circular, elliptical and octagonal CFST columns for the regression analysis are provided in Tables 4, 5 and 6, respectively. The comparison of the ultimate axial strengths determined using Eq. (21) and using the fibre element model is given in Tables 4, 5 and 6. In these tables, $P_{u.design}$ represents the ultimate axial strength determined by utilising Eq. (21). It can be observed from the tables that the ultimate axial strengths predicted using Eq. (21) agree well with numerical results for circular, elliptical and octagonal CFST short columns.

7. Conclusions

The generic confined concrete model for the nonlinear inelastic analysis of circular, elliptical and octagonal CFST short columns under axial loading has been proposed in this paper. The user-defined Python script was developed for conducting the FE model with ABAQUS. The FE model and fibre element model for circular, elliptical and octagonal CFST short columns were verified by comparing the computed results with experimental data. It is demonstrated that the FE model and fibre element model incorporating the generic confined concrete model accurately predicts the ultimate axial strengths and axial load-strain curves for axially loaded circular, elliptical and octagonal CFST short columns. The design model proposed by Liang and Fragomeni (2009) for predicting the ultimate axial strength of circular, elliptical and octagonal CFST short columns was validated. The design model proposed by Liang and Fragomeni (2009) yields accurate predictions of the ultimate axial strengths of axially loaded circular, elliptical and octagonal CFST short columns. Further research is needed to extend the generic confinement model for the concrete core in rectangular, pentagonal and triangular CFST short columns under axial loading, which are being of increasing use in construction.

References

- ACI-318-11 (2011), Building code requirements for structural concrete and commentary ACI Committee 318, Detroit, MI, USA.
- Aslani, F., Uy, B., Tao, Z. and Mashiri, F. (2015a), "Behaviour and design of composite columns incorporating compact high-strength steel plates", *J. Constr. Steel Res.*, **107**, 94-110.
- Aslani, F., Uy, B., Tao, Z. and Mashiri, F. (2015b), "Predicting the axial load capacity of high-strength concrete filled steel tubular columns", *Steel Compos. Struct., Int. J.*, **19**(4), 967-993.
- Dai, X. and Lam, D. (2010), "Numerical modelling of the axial compressive behaviour of short concrete-filled elliptical steel columns", *J. Constr. Steel Res.*, **66**(7), 931-942.
- Ellobody, E. (2013), "A consistent nonlinear approach for analysing steel, cold-formed steel, stainless steel and composite columns at ambient and fire conditions", *Thin-Wall. Struct.*, **68**, 1-17.
- Furlong, R.W. (1967), "Strength of steel-encased concrete beam columns", *J. Struct. Div., ASCE*, **93**(5), 113-124.
- Giakoumelis, G. and Lam, D. (2004), "Axial capacity of circular concrete-filled steel tube columns", *J. Constr. Steel Res.*, **60**(7), 1049-1068.
- Han, L.H., Yao, G.H. and Zhao, X.L. (2005), "Tests and calculations for hollow structural steel (HSS) stub columns filled with self-consolidating concrete (SCC)", *J. Construct. Steel Res.*, **61**(9), 1241-1269.
- Han, L.H., Li, W. and Bjorhovde, R. (2014), "Developments and advanced applications of concrete-filled steel tubular (CFST) structures: Members", *J. Constr. Steel Res.*, **100**, 211-228.
- Hu, H.T., Huang, C.S., Wu, M. and Wu, Y. (2003), "Nonlinear analysis of axially loaded concrete-filled

- tube columns with confinement effect”, *J. Struct. Eng. ASCE*, **129**(10), 1322-1329.
- Jamaluddin, N., Lam, D., Dai, X.H. and Ye, J. (2013), “An experimental study on elliptical concrete filled columns under axial compression”, *J. Construct. Steel Res.*, **87**, 6-16.
- Klöppel, V.K. and Goder, W. (1957), “An investigation of the load carrying capacity of concrete filled steel tubes and development of design formula”, *Der Stahlbau*, **26**(2), 44-50.
- Knowles, R.B. and Park, R. (1969), “Strength of concrete filled steel tubular columns”, *J. Struct. Div., ASCE*, **95**(12), 2565-2588.
- Liang, Q.Q. (2009), “Performance-based analysis of concrete-filled steel tubular beam-columns, Part I: Theory and algorithms”, *J. Constr. Steel Res.*, **65**(2), 363-372.
- Liang, Q.Q. (2014), *Analysis and Design of Steel and Composite Structures*, Boca Raton and London, CRC Press, Taylor and Francis Group.
- Liang, Q.Q. and Fragomeni, S. (2009), “Nonlinear analysis of circular concrete-filled steel tubular short columns under axial loading”, *J. Constr. Steel Res.*, **65**(12), 2186-2196.
- Mander, J.B., Priestly, M.N.J. and Park, R. (1988), “Theoretical stress-strain model for confined concrete”, *J. Struct. Eng. ASCE*, **114**(8), 1804-1826.
- O’Shea, M.D. and Bridge, R.Q. (1998), “Tests on circular thin-walled steel tubes filled with medium and high strength concrete”, *Austral. Civil Eng. Transact.*, **40**, 15-27.
- Patel, V.I., Liang, Q.Q. and Hadi, M.N.S. (2014), “Nonlinear analysis of axially loaded circular concrete-filled stainless steel tubular short columns”, *J. Constr. Steel Res.*, **101**, 9-18.
- Patel, V.I., Liang, Q.Q. and Hadi, M.N.S. (2015), *Nonlinear Analysis of Concrete-Filled Steel Tubular Columns*, Scholars’ Press, Germany.
- Persson, P.O. and Strang, G. (2004), “A simple mesh generator in Matlab”, *SIAM Review*, **46**(2), 329-345.
- Puri, G.M. (2011), *Python Scripts for Abaqus Learn by Example*, Dassault Systèmes Simulia Corporation.
- Ren, Q.X., Han, L.H., Lam, D. and Hou, C. (2014), “Experiments on special-shaped CFST stub columns under axial compression”, *J. Constr. Steel Res.*, **98**, 123-133.
- Richart, F.E., Bradtzaeg, A. and Brown, R.L. (1928), “A study of the failure of concrete under combined compressive stresses”, Bulletin 185, University of Illinois, Engineering Experimental Station, Champaign (III), IL, USA.
- Sakino, K., Nakahara, H., Morino, S. and Nishiyama, I. (2004), “Behavior of centrally loaded concrete-filled steel-tube short columns”, *J. Struct. Eng. ASCE*, **130**(2), 180-188.
- Schneider, S.P. (1998), “Axially loaded concrete-filled steel tubes”, *J. Struct. Eng. ASCE*, **124**(10), 1125-1138.
- Shams, M. and Saadeghvaziri, M.A. (1997), “State of the art of concrete-filled steel tubular columns”, *ACI Struct. J.*, **94**(5), 558-571.
- Shanmugam, N.S. and Lakshmi, B. (2001), “State of the art report on steel-concrete composite columns”, *J. Constr. Steel Res.*, **57**(10), 1041-1080.
- Spacone, E. and El-Tawil, S. (2004), “Nonlinear analysis of steel-concrete composite structures: State of the art”, *J. Struct. Eng. ASCE*, **130**(2), 159-168.
- Susantha, K.A.S., Ge, H.B. and Usami, T. (2001), “Uniaxial stress-strain relationship of concrete confined by various shaped steel tubes”, *Eng. Struct.*, **23**(10), 1331-1347.
- Tang, J., Hino, S., Kuroda, I. and Ohta, T. (1996), “Modeling of stress-strain relationships for steel and concrete in concrete filled circular steel tubular columns”, *Steel Construct. Eng. JSSC*, **3**(11), 35-46.
- Tao, Z., Wang, Z.B. and Yu, Q. (2013), “Finite element modelling of concrete-filled steel stub columns under axial compression”, *J. Constr. Steel Res.*, **89**, 121-131.
- Tomii, M., Yoshimura, K. and Morishita, Y. (1977), “Experimental studies on concrete filled steel tubular stub columns under concentric loading”, *International Colloquium on Stability of Structures under Static and Dynamic Loads*, Washington, D.C., USA, pp. 718-741.
- Uenaka, K. (2014), “Experimental study on concrete filled elliptical/oval steel tubular stub columns under compression”, *Thin-Wall. Struct.*, **78**, 131-137.
- Uy, B., Tao, Z. and Han, L.H. (2011), “Behaviour of short and slender concrete-filled stainless steel tubular columns”, *J. Constr. Steel Res.*, **67**(3), 360-378.

- Yang, H., Lam, D. and Gardner, L. (2008), "Testing and analysis of concrete-filled elliptical hollow sections", *Eng. Struct.*, **30**(12), 3771-3781.
- Zhao, X.L. and Packer, J.A. (2009), "Tests and design of concrete-filled elliptical hollow section stub columns", *Thin-Wall. Struct.*, **47**(6-7), 617-628.

DL